NANO LETTERS

Stochastic Stress Jumps Due to Soliton Dynamics in Two-Dimensional van der Waals Interfaces

SunPhil Kim, Emil Annevelink, Edmund Han, Jaehyung Yu, Pinshane Y. Huang, Elif Ertekin, and Arend M. van der Zande*

Read Online

ACCESS | Metrics & More | Article Recommendations | Supporting Information

ABSTRACT: The creation and movement of dislocations determine the nonlinear mechanics of materials. At the nanoscale, the number of dislocations in structures become countable, and even single defects impact material properties. While the impact of solitons on electronic properties is well studied, the impact of solitons on mechanics is less understood. In this study, we construct nanoelectromechanical drumhead resonators from Bernal stacked bilayer graphene and observe stochastic jumps in frequency. Similar frequency jumps occur in few-layer but not twisted bilayer or monolayer graphene. Using atomistic simulations, we show that the measured shifts are a result of changes in stress due to the creation and annihilation of individual solitons. We develop a simple model relating the magnitude of the stress induced by soliton dynamics across length scales, ranging from <0.01 N/m for the measured 5 μm diameter to ~1.2 N/m for the 38.7 nm simulations. These results demonstrate the sensitivity of 2D resonators are sufficient to probe the nonlinear mechanics of single dislocations in an atomic membrane and provide a model to understand the interfacial mechanics of different kinds of van der Waals structures under stress, which is important to many emerging applications such as engineering quantum states through electromechanical manipulation and mechanical devices like highly tunable nanoelectromechanical systems, stretchable electronics, and origami nanomachines.

KEYWORDS: Solitons, Dislocation, Graphene, NEMS, Nanomechanics, Nonlinear Mechanics
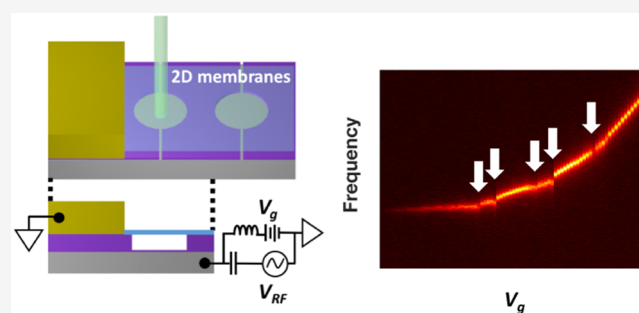
The atomic-scale thickness of two-dimensional (2D) materials like graphene and molybdenum disulfide, combined with their high mechanical strength and flexibility, and excellent electronic properties, open up new opportunities for low power, highly tunable, and highly sensitive nano-electromechanical systems.[1−4] Examples include speakers and microphones from atomic membranes,[5,6] highly tunable filters,[7] oscillators,[8] mass/force sensors,[9,10] and piezotronics.[11] In many cases, micro and nanoelectromechanical systems need more than one layer to connect mechanics to transduction.[12] For example, in 2D material heterostructures, there are now many emerging technologies being explored utilizing mechanical deformations ranging from twistronics[13−15] to origami bimorph nanomachines[16] to deformable electronics from bent[17] or crumpled membranes.[18] In these structures, the weak interlayer bonding and stacking orientation at the van der Waals (vdW) interface dramatically affect the mechanics of 2D membranes and electromechanical coupling, providing a new degree of freedom for engineering 2D mechanical systems. For example, commensurate graphene layers relax interfacial stresses through the presence of solitons, local changes in stacking registry from AB to BA (also known as dislocations or domain walls),[19−21] while twisted or incommensurate

interfaces are superlubric,[14,22] allowing free sliding between layers. Interlayer solitons are mobile, creating and annihilating themselves at high temperatures,[23] under electrostatic field,[24] by a local mechanical stress,[25,26] and their presence leads to changes in local electrical[21] and optical[20] states. These solitons should affect the mechanical properties of the membranes, yet are difficult to measure because of their discrete nature and the lack of techniques to deterministically manipulate them. For example, interlayer shear stress has been measured in bilayer graphene with a pressurized bubble test.[27] Similarly, the inelastic slip between layers in 2D multilayers and heterostructures have been observed through nanoindentation studies, leading to a lower effective elastic modulus[28,29] and conductance modulations.[30] Due to the large forces and low sensitivity, these studies probe the continuum level of many dislocations. Due to their low mass and high tunability, resonators from 2D materials are exceptionally responsive to

perturbations and are being explored as ultrahigh sensitive mass and force sensors.[10,31] Here, we utilize this intrinsic sensitivity to probe the mechanics of 2D interfaces directly and detect the creation and annihilation of a single soliton in bilayer graphene.

In this study, we probe the influence of solitons on the mechanics of 2D membranes by directly comparing the electrostatic tuning of resonance frequency in nanoelectro-mechanical drumhead resonators from CVD grown monolayer graphene (MLG) and commensurate, Bernal stacked bilayer graphene, twisted bilayer graphene, and few-layer graphene. We observe new behaviors in the Bernal stacked bilayer graphene of sudden stochastic jumps in the resonance frequency tuning, which can be either positive or negative, are irreversible and whose magnitude is independent of the initial or electrostatically induced stress of the membrane. Using atomistic simulations, we establish a theory that relates these frequency jumps to changes in stress, resulting from stochastic slip events during the creation and annihilation of solitons. Supporting this theory, twisted bilayer graphene resonators, which have been shown to have superlubric interfaces,[14,22] show no evidence of frequency jumps, while few-layer graphene resonators show many frequency jumps. We develop a simple model relating the magnitude of the stress induced by soliton dynamics across length scales, ranging from <0.01 N/m for the measured 5 μm diameter to ~1.2 N/m for the 38.7 nm simulations. These results demonstrate the sensitivity of 2D resonators is sufficient to probe the nonlinear mechanics of single dislocations in an atomic membrane and provide a model to understand the nonlinear mechanics of different kinds of van der Waals interfaces under stress.

Figure 1a shows a schematic of the 2D material resonators used in this study as well as the electrical circuit used for actuation and tuning. Figure 1b shows a corresponding optical image of one such resonator made from BS-BLG. To fabricate the resonators, 2D atomic membranes composed of monolayer graphene (MLG), Bernal stacked (commensurate) bilayer graphene (BS-BLG), twisted (incommensurate) bilayer graphene (T-BLG), and few-layer graphene (FLG) are transferred and suspended over circular holes with a 5 μm diameter and a depth of 230 nm in a 285 nm thick silicon oxide layer on a degenerately doped silicon substrate (Figure S1). The transferred layer is then electrically contacted by evaporating Cr/Au through a shadow mask (see Supporting Information, Section 1). We use bilayer and few-layer graphene islands grown by chemical vapor deposition.[32] Previous studies have shown these bilayer islands may be either Bernal stacked or twisted, and the Bernal stacked layers contain a higher density of solitons when compared with exfoliated samples.[19,23,33] The use of as-grown bilayer graphene ensures the interface will be atomically clean. In total, we measured 10 resonators including two monolayer graphene (MLG) and three commensurate, Bernal stacked bilayer graphene, two twisted bilayer graphene, and three few-layer graphene. For the majority of the paper, we will focus on the behavior of the BS-BLG and understand the role of the van der Waals interface on the membrane mechanics and then will compare the behavior of other membrane types in Figure 5.

We use Raman spectroscopy and specifically the ratio of the graphene G/2D peaks to confirm the twist angle in the bilayer graphene.[34] Figure 1c is the Raman spectra of both MLG (black) and BLG (red) at the indicated positions in Figure 1b. The monolayer shows a typical graphene Raman spectra with a
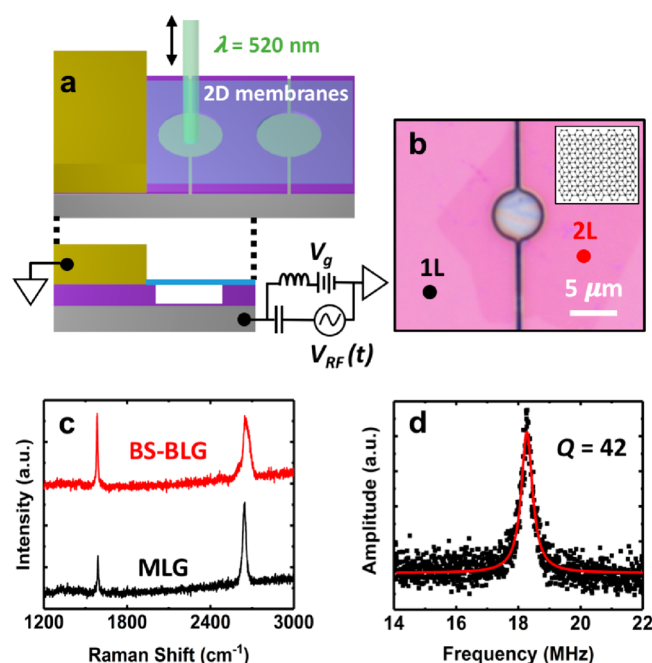

Figure 1. Structure of the 2D material atomic membrane drumhead resonator. (a) Schematic drawing of a suspended 2D membrane circular drumhead resonator and the electronic actuation and optical detection scheme. The suspended membrane is electrostatically actuated, while the mechanical motion is detected by dynamic changes in reflection. (b) An optical image of a Bernal stacked bilayer graphene (BS-BLG) membrane suspended as a 5 μm circular drumhead. The crystal structure is the inset. (c) Raman spectra of monolayer graphene (MLG, black) and Bernal Stacked bilayer graphene (BS-BLG, red), corresponding with the black and red points indicated in panel b. (d) First fundamental resonance of BS-BLG at V_g = 2.4 V, laser power = 50 μW, and V_{RF} = 1 mV.

narrow Lorentzian line shape of the 2D peak with fwhm = 28.6 cm^{-1}, and a 2:1 ratio of 2D to G peak intensities.[34] In contrast, the bilayer shows a reduction in 2D band intensity (2D to G ≅ 1) and a wider 2D peak width, typical of a commensurate bilayer (BS-BLG).[34] Figures S2 and S3 compare the spectroscopic characterization of T-BLG and FLG, respectively, and Figure S4 compares the AFM topography for each membrane type.

To probe the mechanical resonance of the graphene drumhead resonators, we utilize established electrostatic actuation and optical detection techniques,[35−37] shown in Figure 1a and detailed in the Supporting Information, Section 1. Figure 1d shows the first fundamental mode of the BS-BLG resonator from Figure 1b with the Lorentz fit (red) at V_g = 2.4 V. The resonance frequency and the quality factor are 18.2 MHz and 42, respectively, similar to other 2D material drumhead resonators.[1,7,38]

In Figures 2a,b, we compare the electrostatic tuning behavior of monolayer (MLG) and bilayer (BS-BLG) drumhead resonators, respectively. The plots show the dynamic reflected laser response versus DC electrostatic gate voltage V_g and drive frequency. The MLG resonator shown in Figure 2a is well studied in the literature[7,39] and serves as a reference to compare the behavior of the new multilayer structures. Both resonators show frequency tuning, with the electrostatic gate voltage characteristic of atomic membranes. The key difference is the BS-BLG displays discrete jumps in the tuning curve, indicated by white arrows. In contrast, the
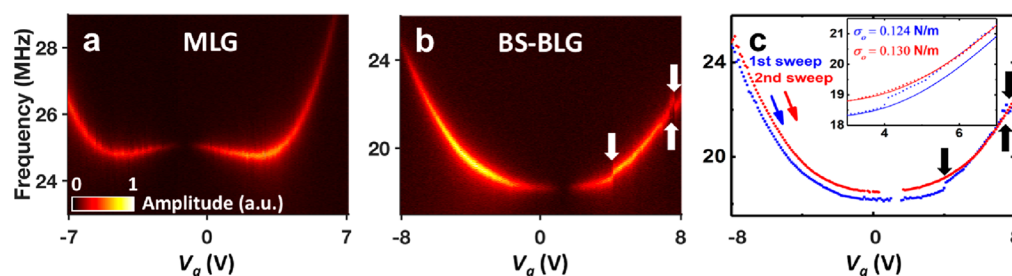
Figure 2. Electrostatic frequency tuning in MLG vs BS-BLG. (a, b) Measured amplitude of motion vs frequency and electrostatic gate voltage for the first fundamental mode of MLG and BS-BLG, respectively. The color scale is the measured dynamic optical reflectance, which is a convolution of the amplitude of motion and changes in the optical interferometric path. Laser power = 50 μW, and V_{RF} = 1 mV. (c) Extracted resonance frequency vs gate voltage for two subsequent sweeps (blue and red) on the same BS-BLG. The first sweep displays frequency jumps, while the second sweep shows no jumps. The inset shows the obtained resonance frequencies from the two subsequent sweeps with a tensioned membrane model fit, yielding the change in the stress of $\Delta\sigma_0$ = 0.006 N/m.
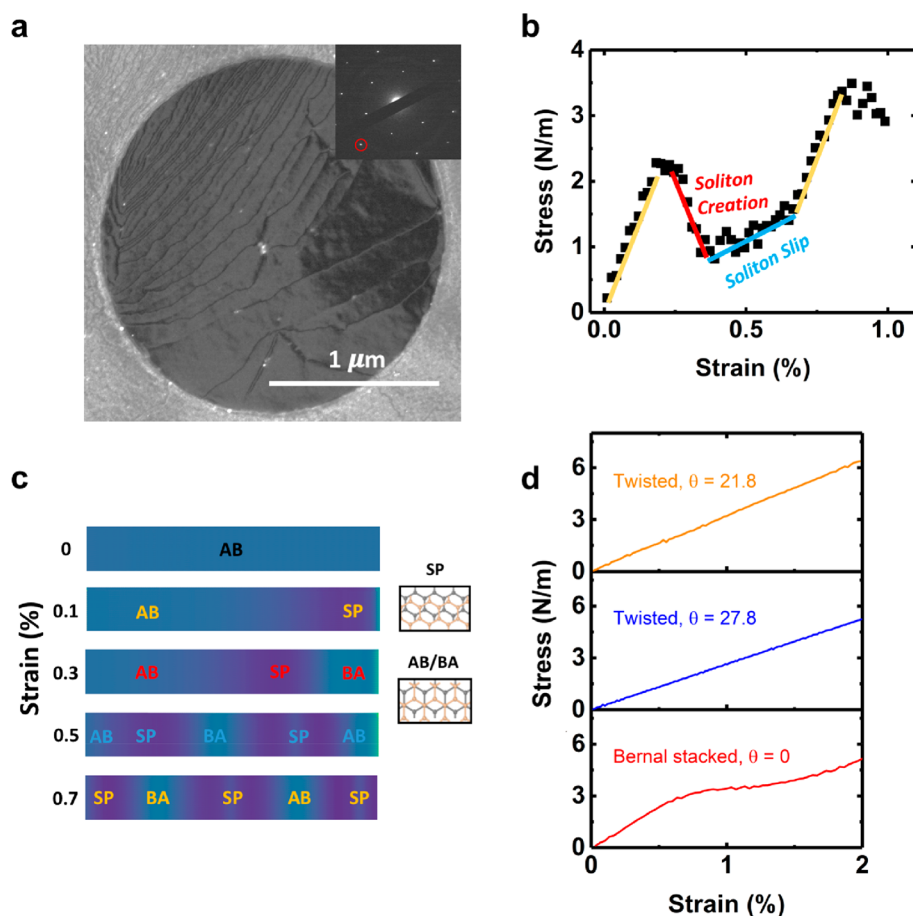
Figure 3. Simulation of solitons in the Bernal Stacked bilayer graphene. (a) DF-TEM image of suspended BS-BLG. Solitons are present, as represented by dark lines. The inset shows the TEM diffraction pattern of BS-BLG. The $\{\bar{2}110\}$ diffraction spots, circled in red, are used for the dark-field imaging. (b) Stress−strain response of a simulated BS-BLG, 38.7 nm in length. The sawtooth steps are a result of the creation of solitons at the interface between the layers. (c) Heatmaps of the BS-BLG at five different strains. The heatmap shows the local registry index within the bilayer with blue corresponding to Bernal stacked AB/BA and purple corresponding to SP-stacking. (d) Stress−strain responses of a 10 nm supercell of BLG with different interlayer twist angles. The underlying linear response dominates the modulus of T-BLG, while dislocation nucleation in BS-BLG alters the modulus, making it appear nonlinear. The smaller supercell size of the BS-BLG in Figure 3d compared with Figure 3b, leads to a higher soliton onset and magnitude, and a more spread out curve. The role of supercell size is detailed further in Figure S10.

MLG resonator displays smooth tuning and is symmetric around the neutral point[7,37] (see also Figure S5). As shown in Figure S6, we have observed similar stochastic frequency jumps in two additional BS-BLG resonators, and sequential scans on the same resonator show additional stochastic jumps with each scan, though not every scan is guaranteed to show a jump. The jumps may be either positive or negative, as seen near $V_g = 4$ and 7 V in Figure 2b. While in Figure 2b, the jumps only occur during tensioning; in the other samples shown in Figure S6, the jumps occur in both the detensioning and tensioning.

First, in Figure 2c, we quantify the mechanics of one jump (the behavior of multiple jumps will be compared later). Figure

2c is a plot of the extracted frequency versus gate voltage for two sequential measurements on the same BS-BLG resonator. Both measurements are taken while sweeping the gate voltage from negative to positive. The blue dotted line represents the first sweep, where a sudden frequency jump of ∼500 kHz is observed at V_g = 4.2 V. The second sweep in red has no large frequency jump. Initially, the tuning in the two measurements is offset by the size of the jump and then is superimposed after the jump occurs. From this, we infer the frequency jumps lead to irreversible and fixed changes in the initial tension of the bilayer.

At the size scales and level of deflection used in this study, mechanically bilayer graphene behaves as a membrane rather than a plate.[40,41] To quantify the change in initial tension due to the stochastic frequency jumps, we apply the tensioned membrane model frequently used to describe the electrostatic tuning of 2D resonators.[1,7,35−39]

$$f_{\mathrm{membrane}}(V_g) = \frac{2.404}{2\pi R}\sqrt{\frac{\sigma_0 + \sigma(V_g)}{\alpha\rho_0}} \qquad (1)$$

In this equation, R is the radius of the membrane, σ_0 is the initial stress in the membrane, $\sigma(V_g)$ is the stress induced by the electrostatic force, ρ_0 is the intrinsic density of the 2D membrane, and α is a factor to account for the additional mass due to adsorbates or polymer residue (Supporting Information, Section 2).

The solid lines in the inset in Figure 2c show the fit to the tensioned membrane model of the first sweep before the frequency jump and to the entire second sweep. From the first sweep, we obtain the density and initial tension of the membrane $\rho = 5.9\rho_0$ and σ_0 = 0.124 N/m, where ρ_0 is the density of pristine BLG. For the second sweep, we assume the same density, resulting in a new initial tension, σ_0 = 0.130 N/m. Hence, the change in stress due to the frequency jump is $\Delta\sigma_0$ = 0.006 N/m, or ∼5% the initial tension in the membrane. We note the tensioned membrane model also takes into account the competition between capacitive softening and electrostatic tensioning, which explains the W versus U shaped tuning curves in the monolayer versus bilayer resonators. These features are well explained in the literature[4] and do not impact the interfacial effects proposed in this study.

We propose the stochastic jumps originate from the introduction and removal of solitons within the tensioned membrane, leading to changes in membrane tension. We also consider and rule out alternative mechanisms for the stochastic jumps in the Supporting Information, Section 3. To support this theory, we performed dark-field transmission electron microscopy (DF-TEM), a diffraction-filtered imaging technique sensitive to changes in stacking order in multilayer graphene, previously used to image grain boundaries and solitons in graphene and other 2D materials.[19,23] Figure 3a is a DF-TEM image of a BS-BLG suspended over a hole in a TEM grid. The graphene imaged is fabricated from the same growth used to generate the bilayer resonators. The inset diffraction pattern shows the bilayer graphene is a single crystal and Bernal stacked, with a single set of 6-fold symmetric spots. By using an objective aperture to select the $\{\overline{2}110\}$ diffraction spot, we produce the image in Figure 3a. Here the bright regions are Bernal stacked bilayers, with either AB or BA stacking orders. The locations of solitons are shown as dark lines and correspond with a transition between stacking orders AB to BA or vice versa.[19,23] The image shows the graphene

membranes contain many solitons (here, several dozen in a 4 square micron area), even before the introduction of electrostatic tension. We observed a similar density of solitons in other Bernal stacked regions on this sample, although the soliton number, shape, and size vary; two additional bilayer regions are shown in Figure S7. Figure S8 shows a third region captured using the $\{\overline{1}010\}$ diffraction spot, which shows the solitons correspond with changes in stacking order.

To understand the impact of the interlayer solitons on the mechanical properties of graphene resonators, we carry out LAMMPS[42] molecular statics simulations of bilayer graphene, wherein one layer is tensioned and the other layer is free to relax (Supporting Information, Section 4, and Figure S9). Figure 3b shows the stress response of a simulated 38.7 nm supercell of BS-BLG under uniaxial tensile strain. The stress−strain response has a sawtooth shape, with regions of different elastic moduli, indicated by lines of different colors. To explain the origin of the sawtooth features, Figure 3c shows the atomic stacking at five different tensile strains as a heatmap of the local registry index (LRI).[43] At zero strain, the stacking is AB everywhere. At small strains, <0.2% (yellow), the two layers are almost uniformly strained, leading to an elastic modulus of ∼1000 N/m, which is higher than the elastic modulus of BLG. The higher effective modulus is a result of the interaction energy between dislocations, which depends on dislocation separation and, thus, on the periodicity of the simulations. Figure S10 quantifies the dependence of the nucleation strain with a supercell size as well as an interlayer twist, described below. Between 0.2 and 0.4% strain (red), the stress−strain curve is negative, corresponding with the layers breaking registry as the crossing of a Peierls barrier results in the nucleation of a soliton[23,44] and a region of BA stacking. Next, between 0.4 and 0.7% strain (blue), the elastic modulus corresponds to a single layer in tension ∼340 N/m.[45] The LRI at 0.5% strain shows the nucleation of a second dislocation. The pair of dislocations accommodate misregistry and prevent the transfer of strain between the layers. At 0.7% strain, the process repeats.

These simulations also compare the relative response of Bernal stacked and twisted bilayer graphene. Figure 3d uses the stress−strain response to show the difference of interfacial properties of twisted to Bernal stacked graphene. Figure 3d compares simulated stress responses for a supercell of 100 Å of BS- and T-BLG (θ = 21.8 and 27.8) under uniaxial tension. The modulus changes of the BS-BLG correspond to the nucleation of solitons. In contrast, twisted bilayer graphene is an array of screw dislocation and solitons as a partial edge dislocation in which there is a local change in the periodicity of the moiré superlattice.[44] These screw dislocations have much smaller Burgers vectors than aligned layers and have a much lower Peierls barrier height. As a result, there is no observable sawtooth pattern in the simulated twisted bilayer under stress. This nearly linear modulus of T-BLG is a signature of superlubricity, which is the result of the lower commensurability of the twisted structures. The smaller simulation supercell size of the BS-BLG in Figure 3d compared to Figure 3b leads to a larger onset and magnitude of the steps in stress−strain response. The role of supercell size is detailed further in Figure S10.

Using the atomic-scale simulations as a guide, Figure 4a describes the impact of soliton creation, annihilation, and slip on the resonance frequency. Soliton creation is a result of a localized change in stacking order or slip of soliton from the
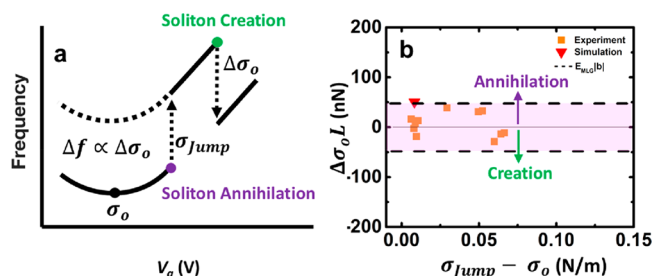
Figure 4. Impact of solitons on resonator stress. (a) Illustration of how the creation and annihilation of solitons will impact the frequency of the resonators, and the relations of stress to frequency and change in frequency ($\Delta f \propto \Delta\sigma_0$). (b) Plot of the size normalized magnitude of stress jumps $\Delta\sigma_0 L$ versus the stress at which a jump occurs. Orange squares are the changes in stress extracted from multiple sweeps in 3 separate BS-BLG resonators; the red point is the value predicted from the simulation. The dashed lines represent the theoretically predicted value for the creation or annihilation of a single soliton.

edges. Soliton annihilation is caused by either the recombination of two different stacking orders in the membrane or the exit of an existing soliton through the edges. As seen in Figure 3b, creating a soliton will increase the overall length of the resonator, leading to a decrease in the stress and a drop in frequency. In reverse, annihilating solitons will decrease the overall length, leading to an increase in overall stress and a rise in frequency. Soliton slip, wherein the soliton changes position in the membrane, does not change the effective length, so it will not lead to observable discrete changes in stress unless the slip is completely off the edge of the membrane. However, the slip may rearrange or bring existing solitons together, enabling annihilation of existing solitons or separation of newly created solitons. Because each suspended membrane has a different random network of solitons, the exact tension or gate voltage at which these events will occur will vary sample to sample and depend on the history of gating.

Next, we discuss how to relate the atomistic simulations to the micron scale resonators quantitatively. First, the simulations are quasistatic calculations of stress at fixed strains, whereas the electrostatically gated resonators are a fixed force system. As a result, while the simulations show a slow change in the stress versus strain for the introduction of a soliton, the resonators show a sudden jump due to the balancing of the forces. Second, the effective stress induced by the addition of a single dislocation will depend on system size. This may be explained by considering that the change in energy by the creation of a single soliton is related to a fixed change in length of one layer stretching over the other layer by the Burgers vector $|b|$. The change in length is accommodated by the entire membrane, thus giving a change in stress of

$$\Delta\sigma_0 = \pm E_{MLG}\frac{|b|}{L} \qquad (2)$$

where $|b| = 1.42$ Å is the Burgers vector of the tensile soliton in the zigzag direction,[23] and $E_{MLG} = 340$ N/m is the monolayer elastic modulus.[45] L is the length of the stretched membrane accommodating the strain (38.7 nm for the simulation or 5 μm for the diameter of the drumhead membranes).

In Figure 4, we apply eq 2 to compare the size normalized impact of solitons on stress for both experiment and simulation. Figure 4b plots $\Delta\sigma_0 L$ versus the relative stress at which the jump occurs in experiments, simulation, and theory.

Physically, the size-independent $\Delta\sigma_0 L$ can be interpreted as the work done to create a soliton per unit width. The orange points are the experimentally derived values from multiple sweeps on 3 different BS-BLG resonators (Figure S6); the red point is the value extracted from the simulation in Figure 3b and Figure S10, and the dashed lines indicate the theoretical value $E_{MLG}|b| \approx 48.3$ nN predicted from eq 2, assuming a soliton spans the entire length of a system. We are comparing multiple resonators and systems with a different initial stress, so the x-axis is plotted as the change in stress at the onset of soliton dynamics ($\sigma_{jump} - \sigma_0$), where σ_{jump} is the stress just before the frequency jump.

From Figure 4b, the simulated value for soliton creation agrees very well with the theoretical value from eq 2. Experimentally, we observe both positive and negative jumps in the frequency and thereby both positive and negative changes in stress. Yet, the magnitude of the jumps is always within the range of values predicted for the creation or annihilation of a single soliton (pink region) or |$\Delta\sigma_0 L$|< 48.3 nN. The measured values are all on the same order but smaller than the theory because, (1) as seen in Figure 3a, most solitons are randomly distributed in size and orientation throughout the membrane, and (2) the stress changes from an individual soliton will be uniaxial, while we measure the effective biaxial stress in the membranes.

Finally, we apply the same approach to drumhead membranes made from other 2D interfaces, namely, twisted bilayer graphene and Bernal stacked few-layer graphene. Figure 5a,b shows the electrostatic tuning curves of T-BLG and FLG,
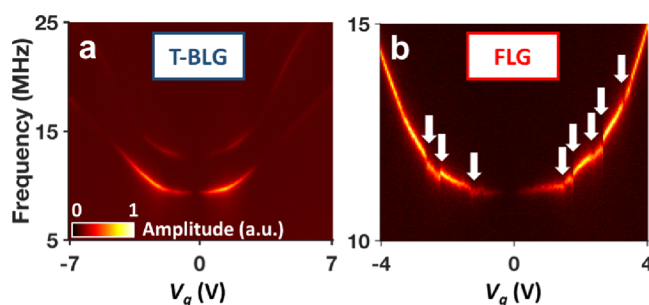
Figure 5. Tuning behavior in other 2D interfaces. (a, b) Frequency vs gate voltage electrostatic tuning curves for (a) T-BLG and (b) FLG. T-BLG shows an absence of frequency jumps, while FLG displays many more frequency jumps than Bernal stacked bilayer graphene.

respectively. In Figure 5a, the tuning curve for T-BLG is smooth, with no visible frequency jumps. In contrast, in Figure 5b, the tuning curve for FLG displays a more complex behavior with many more frequency jumps. These observations are consistent with our model. According to Figure 3 and previous measurements demonstrating low friction in twisted graphite,[14,22] the magnitude of any changes in stress should be below the threshold of measurement in twisted interfaces. In contrast, FLG has multiple Bernal stacked interfaces, leading to more opportunities for soliton creation/annihilation to occur. Figures S11 and 12 show consistent behavior in additional T-BLG and FLG resonators. In Figure S13, we directly compare the relative magnitude of the frequency jumps in the different membrane types and find the magnitude of events in both systems are very similar.

In conclusion, we observed discrete and stochastic frequency jumps in the tuning curves from BS-BLG resonators,

corresponding to irreversible changes in the initial tension of the membranes. We propose a model of soliton creation and annihilation to explain the frequency jumps. We extend the measurement to find similar frequency jumps in few-layer graphene, but not twisted bilayers. These results provide a foundation to understand and directly probe the mechanics of other vdW interfaces in 2D heterostructures, which will be important to engineering mechanically active devices from 2D heterostructures with applications such as stochastic switching[46] driven by soliton dynamics, electromechanical control of topological states, and engineering the stiffness in 3D structures from 2D materials like crumpled electronics[18] and origami nanomachines.[16,47]

■ ASSOCIATED CONTENT

Supporting Information

The Supporting Information is available free of charge at https://pubs.acs.org/doi/10.1021/acs.nanolett.9b04619.

Methods on resonator fabrication, bilayer identification, optomechanical measurements, atomic simulation, and dark-field electron microscopy, details on the tensioned membrane model, discussion and elimination of alternate mechanisms that may generate frequency jumps, and simulation parameters (PDF)

■ AUTHOR INFORMATION

Corresponding Author

Arend M. van der Zande − *University of Illinois at Urbana−Champaign, Urbana, Illinois;* orcid.org/0000-0001-5104-9646; Phone: 217-244-2912; Email: arendv@illinois.edu

Other Authors

SunPhil Kim − *University of Illinois at Urbana−Champaign, Urbana, Illinois;* orcid.org/0000-0002-5627-1139

Emil Annevelink − *University of Illinois at Urbana−Champaign, Urbana, Illinois*

Edmund Han − *University of Illinois at Urbana−Champaign, Urbana, Illinois*

Jaehyung Yu − *University of Illinois at Urbana−Champaign, Urbana, Illinois;* orcid.org/0000-0002-9925-2309

Pinshane Y. Huang − *University of Illinois at Urbana−Champaign, Urbana, Illinois;* orcid.org/0000-0002-1095-1833

Elif Ertekin − *University of Illinois at Urbana−Champaign, Urbana, Illinois;* orcid.org/0000-0002-7816-1803

Complete contact information is available at:
https://pubs.acs.org/10.1021/acs.nanolett.9b04619

Author Contributions

A.M.v.d.Z and S.P.K. conceived and implemented the project. Under A.M.v.d.Z's supervision, S.P.K. performed sample fabrication, resonator measurements, and mechanical analysis. J.H.Y. assisted in sample fabrication. Under E.E.'s supervision, E.A. performed the classical potential simulations. Under P.Y.H.'s supervision, E.H. performed dark-field transmission electron microscopy. A.M.v.d.Z and S.P.K wrote the manuscript. All authors read and contributed to the manuscript.

Notes

The authors declare no competing financial interest.

■ ACKNOWLEDGMENTS

■ REFERENCES

(1) Bunch, J. S.; van der Zande, A. M.; Verbridge, S. S.; Frank, I. W.; Tanenbaum, D. M.; Parpia, J. M.; Craighead, H. G.; McEuen, P. L. Electromechanical resonators from graphene sheets. *Science* **2007**, *315* (5811), 490−493.

(2) Akinwande, D.; Brennan, C. J.; Bunch, J. S.; Egberts, P.; Felts, J. R.; Gao, H. J.; Huang, R.; Kim, J. S.; Li, T.; Li, Y.; Liechti, K. M.; Lu, N. S.; Park, H. S.; Reed, E. J.; Wang, P.; Yakobson, B. I.; Zhang, T.; Zhang, Y. W.; Zhou, Y.; Zhu, Y. A review on mechanics and mechanical properties of 2D materials-Graphene and beyond. *Extrem. Mech. Lett.* **2017**, *13*, 42−77.

(3) Barton, R. A.; Parpia, J.; Craighead, H. G. Fabrication and performance of graphene nanoelectromechanical systems. *J. Vac. Sci. Technol., B: Nanotechnol. Microelectron.: Mater., Process., Meas., Phenom.* **2011**, *29* (5), 050801.

(4) Chen, C. Y.; Hone, J. Graphene Nanoelectromechanical Systems. *Proc. IEEE* **2013**, *101* (7), 1766−1779.

(5) Zhou, Q.; Zettl, A. Electrostatic graphene loudspeaker. *Appl. Phys. Lett.* **2013**, *102* (22), 223109.

(6) Zhou, Q.; Zheng, J. L.; Onishi, S.; Crommie, M. F.; Zettl, A. K. Graphene electrostatic microphone and ultrasonic radio. *Proc. Natl. Acad. Sci. U. S. A.* **2015**, *112* (29), 8942−8946.

(7) van der Zande, A. M.; Barton, R. A.; Alden, J. S.; Ruiz-Vargas, C. S.; Whitney, W. S.; Pham, P. H.; Park, J.; Parpia, J. M.; Craighead, H. G.; McEuen, P. L. Large-scale arrays of single-layer graphene resonators. *Nano Lett.* **2010**, *10* (12), 4869−4873.

(8) Chen, C.; Lee, S.; Deshpande, V. V.; Lee, G. H.; Lekas, M.; Shepard, K.; Hone, J. Graphene mechanical oscillators with tunable frequency. *Nat. Nanotechnol.* **2013**, *8* (12), 923−927.

(9) Chen, C.; Rosenblatt, S.; Bolotin, K. I.; Kalb, W.; Kim, P.; Kymissis, I.; Stormer, H. L.; Heinz, T. F.; Hone, J. Performance of monolayer graphene nanomechanical resonators with electrical readout. *Nat. Nanotechnol.* **2009**, *4* (12), 861−867.

(10) Weber, P.; Guttinger, J.; Noury, A.; Vergara-Cruz, J.; Bachtold, A. Force sensitivity of multilayer graphene optomechanical devices. *Nat. Commun.* **2016**, *7*, 12496.

(11) Wu, W.; Wang, L.; Li, Y.; Zhang, F.; Lin, L.; Niu, S.; Chenet, D.; Zhang, X.; Hao, Y.; Heinz, T. F.; Hone, J.; Wang, Z. L. Piezoelectricity of single-atomic-layer MoS2 for energy conversion and piezotronics. *Nature* **2014**, *514* (7523), 470−474.

(12) Li, H. D.; Tian, C.; Deng, Z. D. Energy harvesting from low frequency applications using piezoelectric materials. *Appl. Phys. Rev.* **2014**, *1* (4), 041301.

(13) Ribeiro-Palau, R.; Zhang, C. J.; Watanabe, K.; Taniguchi, T.; Hone, J.; Dean, C. R. Twistable electronics with dynamically rotatable heterostructures. *Science* **2018**, *361* (6403), 690−693.

(14) Koren, E.; Lortscher, E.; Rawlings, C.; Knoll, A. W.; Duerig, U. Adhesion and friction in mesoscopic graphite contacts. *Science* **2015**, *348* (6235), 679−683.

(15) Koren, E.; Leven, I.; Lortscher, E.; Knoll, A.; Hod, O.; Duerig, U. Coherent commensurate electronic states at the interface between misoriented graphene layers. *Nat. Nanotechnol.* **2016**, *11* (9), 752−757.

(16) Miskin, M. Z.; Dorsey, K. J.; Bircan, B.; Han, Y.; Muller, D. A.; McEuen, P. L.; Cohen, I. Graphene-based bimorphs for micron-sized, autonomous origami machines. *Proc. Natl. Acad. Sci. U. S. A.* **2018**, *115* (3), 466−470.

(17) Lee, G. H.; Yu, Y. J.; Cui, X.; Petrone, N.; Lee, C. H.; Choi, M. S.; Lee, D. Y.; Lee, C.; Yoo, W. J.; Watanabe, K.; Taniguchi, T.; Nuckolls, C.; Kim, P.; Hone, J. Flexible and Transparent MoS2 Field-Effect Transistors on Hexagonal Boron Nitride-Graphene Heterostructures. *ACS Nano* **2013**, *7* (9), 7931−7936.

(18) Kang, P.; Wang, M. C.; Knapp, P. M.; Nam, S. Crumpled Graphene Photodetector with Enhanced, Strain-Tunable, and Wavelength-Selective Photoresponsivity. *Adv. Mater.* **2016**, *28* (23), 4639−4645.

(19) Butz, B.; Dolle, C.; Niekiel, F.; Weber, K.; Waldmann, D.; Weber, H. B.; Meyer, B.; Spiecker, E. Dislocations in bilayer graphene. *Nature* **2014**, *505* (7484), 533−537.

(20) Jiang, L. L.; Shi, Z. W.; Zeng, B.; Wang, S.; Kang, J. H.; Joshi, T.; Jin, C. H.; Ju, L.; Kim, J.; Lyu, T.; Shen, Y. R.; Crommie, M.; Gao, H. J.; Wang, F. Soliton-dependent plasmon reflection at bilayer graphene domain walls. *Nat. Mater.* **2016**, *15* (8), 840−844.

(21) Ju, L.; Shi, Z. W.; Nair, N.; Lv, Y. C.; Jin, C. H.; Velasco, J.; Ojeda-Aristizabal, C.; Bechtel, H. A.; Martin, M. C.; Zettl, A.; Analytis, J.; Wang, F. Topological valley transport at bilayer graphene domain walls. *Nature* **2015**, *520* (7549), 650−655.

(22) Dienwiebel, M.; Verhoeven, G. S.; Pradeep, N.; Frenken, J. W. M.; Heimberg, J. A.; Zandbergen, H. W. Superlubricity of graphite. *Phys. Rev. Lett.* **2004**, *92* (12), 126101.

(23) Alden, J. S.; Tsen, A. W.; Huang, P. Y.; Hovden, R.; Brown, L.; Park, J.; Muller, D. A.; McEuen, P. L. Strain solitons and topological defects in bilayer graphene. *Proc. Natl. Acad. Sci. U. S. A.* **2013**, *110* (28), 11256−11260.

(24) Yankowitz, M.; Wang, J. I. J.; Birdwell, A. G.; Chen, Y. A.; Watanabe, K.; Taniguchi, T.; Jacquod, P.; San-Jose, P.; Jarillo-Herrero, P.; LeRoy, B. J. Electric field control of soliton motion and stacking in trilayer graphene. *Nat. Mater.* **2014**, *13* (8), 786−789.

(25) Schweizer, P.; Dolle, C.; Spiecker, E. In situ manipulation and switching of dislocations in bilayer graphene. *Sci. Adv.* **2018**, *4* (8), No. eaat4712.

(26) Jiang, L. L.; Wang, S.; Shi, Z. W.; Jin, C. H.; Utama, M. I. B.; Zhao, S. H.; Shen, Y. R.; Gao, H. J.; Zhang, G. Y.; Wang, F. Manipulation of domain-wall solitons in bi- and trilayer graphene. *Nat. Nanotechnol.* **2018**, *13* (3), 204−208.

(27) Wang, G. R.; Dai, Z. H.; Wang, Y. L.; Tan, P. H.; Liu, L. Q.; Xu, Z. P.; Wei, Y. G.; Huang, R.; Zhang, Z. Measuring Interlayer Shear Stress in Bilayer Graphene. *Phys. Rev. Lett.* **2017**, *119* (3), 036101.

(28) Liu, K.; Yan, Q. M.; Chen, M.; Fan, W.; Sun, Y. H.; Suh, J.; Fu, D. Y.; Lee, S.; Zhou, J.; Tongay, S.; Ji, J.; Neaton, J. B.; Wu, J. Q. Elastic Properties of Chemical-Vapor-Deposited Monolayer MoS2, WS2, and Their Bilayer Heterostructures. *Nano Lett.* **2014**, *14* (9), 5097−5103.

(29) Wei, X. D.; Meng, Z. X.; Ruiz, L.; Xia, W. J.; Lee, C.; Kysar, J. W.; Hone, J. C.; Keten, S.; Espinosa, H. D. Recoverable Slippage Mechanism in Multilayer Graphene Leads to Repeatable Energy Dissipation. *ACS Nano* **2016**, *10* (2), 1820−1828.

(30) Benameur, M. M.; Gargiulo, F.; Manzeli, S.; Autes, G.; Tosun, M.; Yazyev, O. V.; Kis, A. Electromechanical oscillations in bilayer graphene. *Nat. Commun.* **2015**, *6*, 8582.

(31) Chaste, J.; Eichler, A.; Moser, J.; Ceballos, G.; Rurali, R.; Bachtold, A. A nanomechanical mass sensor with yoctogram resolution. *Nat. Nanotechnol.* **2012**, *7* (5), 301−303.

(32) Fang, W. J.; Hsu, A. L.; Song, Y.; Kong, J. A review of large-area bilayer graphene synthesis by chemical vapor deposition. *Nanoscale* **2015**, *7* (48), 20335−20351.

(33) Havener, R. W.; Zhuang, H.; Brown, L.; Hennig, R. G.; Park, J. Angle-resolved Raman imaging of interlayer rotations and interactions in twisted bilayer graphene. *Nano Lett.* **2012**, *12* (6), 3162−3167.

(34) Ferrari, A. C.; Basko, D. M. Raman spectroscopy as a versatile tool for studying the properties of graphene. *Nat. Nanotechnol.* **2013**, *8* (4), 235−246.

(35) Kim, S.; Yu, J.; van der Zande, A. M. Nano-electromechanical Drumhead Resonators from Two-Dimensional Material Bimorphs. *Nano Lett.* **2018**, *18*, 6686−6695.

(36) Morell, N.; Reserbat-Plantey, A.; Tsioutsios, I.; Schadler, K. G.; Dubin, F.; Koppens, F. H.; Bachtold, A. High Quality Factor Mechanical Resonators Based on WSe2Monolayers. *Nano Lett.* **2016**, *16* (8), 5102−5108.

(37) Weber, P.; Guttinger, J.; Tsioutsios, I.; Chang, D. E.; Bachtold, A. Coupling Graphene Mechanical Resonators to Superconducting Microwave Cavities. *Nano Lett.* **2014**, *14* (5), 2854−2860.

(38) Lee, J.; Wang, Z.; He, K.; Yang, R.; Shan, J.; Feng, P. X. Electrically tunable single- and few-layer MoS2 nanoelectromechanical systems with broad dynamic range. *Sci. Adv.* **2018**, *4* (3), No. eaao6653.

(39) Barton, R. A.; Storch, I. R.; Adiga, V. P.; Sakakibara, R.; Cipriany, B. R.; Ilic, B.; Wang, S. P.; Ong, P.; McEuen, P. L.; Parpia, J. M.; Craighead, H. G. Photothermal Self-Oscillation and Laser Cooling of Graphene Optomechanical Systems. *Nano Lett.* **2012**, *12* (9), 4681−4686.

(40) Wang, G. R.; Dai, Z. H.; Xiao, J. K.; Feng, S. Z.; Weng, C. X.; Liu, L. Q.; Xu, Z. P.; Huang, R.; Zhang, Z. Bending of Multilayer van der Waals Materials. *Phys. Rev. Lett.* **2019**, *123* (11), 116101.

(41) Lee, J.; Wang, Z. H.; He, K. L.; Shan, J.; Feng, P. X. L. High Frequency MoS2 Nanomechanical Resonators. *ACS Nano* **2013**, *7* (7), 6086−6091.

(42) Plimpton, S. Fast Parallel Algorithms for Short-Range Molecular-Dynamics. *J. Comput. Phys.* **1995**, *117* (1), 1−19.

(43) Leven, I.; Guerra, R.; Vanossi, A.; Tosatti, E.; Hod, O. Multiwalled nanotube faceting unravelled. *Nat. Nanotechnol.* **2016**, *11* (12), 1082−1086.

(44) Pochet, P.; McGuigan, B. C.; Coraux, J.; Johnson, H. T. Toward Moire engineering in 2D materials via dislocation theory. *Appl. Mater. Today* **2017**, *9*, 240−250.

(45) Lee, C.; Wei, X. D.; Kysar, J. W.; Hone, J. Measurement of the elastic properties and intrinsic strength of monolayer graphene. *Science* **2008**, *321* (5887), 385−388.

(46) Dolleman, R. J.; Belardinelli, P.; Houri, S.; van der Zant, H. S. J.; Alijani, F.; Steeneken, P. G. High-Frequency Stochastic Switching of Graphene Resonators Near Room Temperature. *Nano Lett.* **2019**, *19* (2), 1282−1288.

(47) Blees, M. K.; Barnard, A. W.; Rose, P. A.; Roberts, S. P.; McGill, K. L.; Huang, P. Y.; Ruyack, A. R.; Kevek, J. W.; Kobrin, B.; Muller, D. A.; McEuen, P. L. Graphene kirigami. *Nature* **2015**, *524* (7564), 204−207.